Effects of boundary slips on thermal elastohydrodynamic lubrication under pure rolling and opposite sliding contacts

Xianghua Meng [a], Jing Wang [b], Hiroshi Nishikawa [c], Gyoko Nagayama [c, *]

[a] Graduate School of Engineering, Kyushu Institute of Technology, 8048550, Fukuoka, Japan

[b] College of Mechanical Engineering, Donghua University, 201620, Shanghai, China

[c] Department of Mechanical Engineering, Kyushu Institute of Technology, 8048550, Fukuoka, Japan

Abstract: In elastohydrodynamic lubrication (EHL) contact, the film thickness strongly depends on boundary slips, including velocity slip and thermal slip at the solid–lubricant interface. In the EHL studies published thus far, velocity slip at the solid–lubricant interface has been investigated individually without considering thermal slip. In this study, the effects of both types of boundary slip on film thickness were investigated simultaneously in rolling/sliding contact. Numerical simulations were conducted based on the modified Reynolds equation and energy equation by considering boundary slips on the sliding surface. The results indicate that the velocity slip causes a reduction in film thickness under pure rolling contact, while a shifted surface dimple is formed along the sliding direction due to both velocity slip and thermal slip under zero entrainment velocity (ZEV) contact.

Keywords: Slip length, Thermal slip length, Slip boundary condition, Thermal elastohydrodynamic lubrication.

* Corresponding author.

E-mail address: nagayama@mech.kyutech.ac.jp

1 Introduction

In the elastohydrodynamic lubrication (EHL) regime, the no-slip boundary condition has been commonly accepted for many years. However, with the recent technical advances in interface sciences, the slip boundary condition has attracted the attention of EHL researchers. According to the no-slip boundary hypothesis, both the velocity and temperature of the lubricant adjacent to the solid surface are the same as those of the solid surface [1–3], while the slip boundary includes a velocity discontinuity and a temperature jump at the solid–lubricant interface [4–8] The slip boundary condition plays a vital role in lubrication analyses, especially in the two typical rolling/sliding contacts of (a) pure rolling and (b) zero entrainment velocity (ZEV), as shown in Fig. 1. The velocity discontinuity shown in Fig. 1 (c) can be described in terms of slip length, which is defined as the distance between the solid–lubricant interface and the position at which the lubricant velocity and solid velocity are equal [4,6]. Analogously, the temperature jump shown in Fig. 1 (c) can be determined using the thermal slip length, which is the distance from the interface to the position at which the temperature difference between the lubricant and solid is zero [7–10].

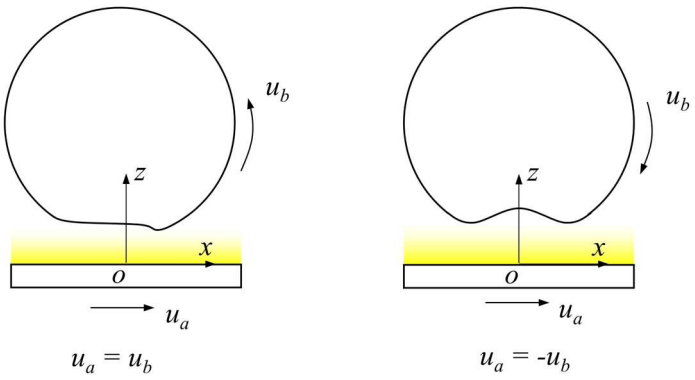

(a) Pure rolling contact (b) ZEV contact

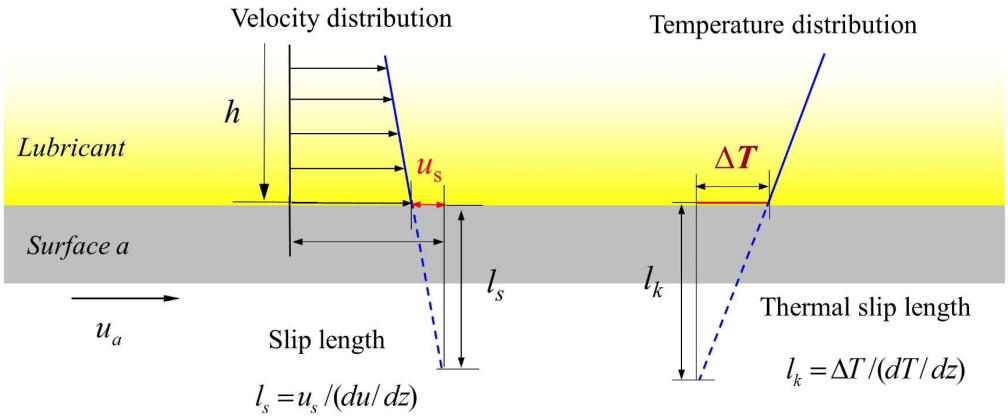

(c) Slip boundary condition on surface *a*

Fig. 1 Schematic of (a) pure rolling contact, (b) ZEV contact, and (c) slip boundary condition at surface *a*.

Velocity discontinuity at the interface is one of the most important features considered in EHL analyses. Kaneta et al. [11] reported that a lubricant film behaved like a solid and slipped at the interface in EHL contact. Wong et al. [12] performed a series of optical interferometry experiments to gather evidence of the velocity slip based on the relative movement of the lubricant entrapped in the contact area. Ponjavic and Wong [13] used the photobleached-fluorescence imaging velocimetry technique to measure slip under steady conditions and found that friction and film thickness decreased due to the velocity slip in EHL contact. In the experiments of Wang and Reddyhoff [14], an anomalous EHL film shape was obtained by using the lubricant 1-dodecanol. They hypothesized that the velocity slip that occurred at the interface caused an increase in film thickness to maintain flow continuity. Moreover, theoretical models with the velocity slip assumption have been developed for EHL contacts. Ehret et al. [15] proposed a plug flow model for the EHL regime with an interfacial slip assumption and demonstrated the formation of a surface dimple under the sliding condition. The results of a molecular dynamics simulation performed by Nagayama et al. [16,17] indicated that the solid–liquid boundary condition depends on the interface wettability and the driving force for liquid flow in a nanochannel. Wen and Zhang [18], as well as Chu et al. [19], proposed an ideal

viscoplastic rheological model for isothermal EHL line contact with velocity boundary slippage, and this model yielded considerably thinner films than those obtained using the no-slip theory. Chen et al. [20] investigated the effect of anisotropic velocity slip on pressure and film distributions under point EHL contacts. Furthermore, Zhao et al. [21] conducted a thermal point EHL analysis to investigate the coupled effects of velocity slip and heat transfer. They found that the velocity slip at the interface constrained temperature rise and increased film thickness under large slide-roll ratio conditions.

In addition to the aforementioned boundary slips, the surface sliding direction can influence the lubrication performance in the EHL regime. When two bounding surfaces have equal but opposite velocities (known as ZEV contact), the working condition may be the most severe for ball screws or roller bearings without a cage. Cameron [22,23] first described film formation under ZEV contact and proposed the viscosity wedge theory to demonstrate the viscosity variations induced by the temperature gradient across the lubricant film. Yang et al. [24] renamed Cameron's viscosity wedge theory as the "temperature-viscosity wedge" mechanism to highlight the importance of temperature rise. The complete numerical solutions obtained by Guo et al. [25,26] indicated that the film shape in the contact area was characterized by a deep central dimple, which was mainly ascribed to the temperature-viscosity wedge effect. Yagi et al. [27] measured the temperature distribution in the dimple zone, and their results indicated that the maximum temperature occasionally reached 400 K. In addition, Meziane et al. [28] found the results of numerical simulations, including thermal effects, agreed with the experimental results, thus allowing for tentative prediction of the minimum film thickness in wide-point EHL contact. Zhang et al. [29,30] theoretically investigated surface dimple variations and found that the existence of the surface dimple was related to the temperature rise under ZEV contact. Considering the reasonable doubts about the no-slip boundary conditions applied in previous studies, Wong et al. [31,32] fabricated oleophobic/oleophilic surfaces under

ZEV contact with extremely low surface velocity, where a considerable velocity slip might occur at the solid–lubricant interface.

Although the velocity slip of EHL contact has been studied extensively, few comparisons have been made between experimental and simulation data. Moreover, thermal slip has been rarely coupled with velocity slip in the existing studies, especially under ZEV contact. Hence, in this study, the effects of velocity slip and thermal slip on lubrication were investigated simultaneously under the pure rolling and ZEV contacts. Numerical simulations were conducted based on a modified Reynolds equation and the energy equation by considering the two types of boundary slips on a sliding surface.

2 Governing equations

Considering the pure rolling contact and ZEV contact shown in Fig. 1, the slip boundary conditions shown in Fig. 1 (c) were applied to surface *a*, on which both velocity slip and thermal slip occur, and the continuum boundary condition was applied to surface *b*. According to the linear Navier boundary condition [4–6] the slip velocity at an interface is proportional to the slip length:

$$u_s = l_s \left.\frac{\partial u}{\partial z}\right|_{z=0}. \tag{1}$$

The thermal slip accompanying the velocity slip can be expressed as follows [7]:

$$\Delta T = l_k \left.\frac{\partial T}{\partial z}\right|_{z=0}. \tag{2}$$

For the thermal point EHL contact, the modified Reynolds equation accounting for boundary slips on one surface is derived based on the generalized Reynolds equation [33]:

$$\frac{\partial}{\partial x}\left[\left(\frac{\rho}{\eta}\right)_{es} h^3 \frac{\partial p}{\partial x}\right] + \frac{\partial}{\partial x}\left[\left(\frac{\rho}{\eta}\right)_{e} h^3 \frac{\partial p}{\partial x}\right] + \frac{\partial}{\partial y}\left[\left(\frac{\rho}{\eta}\right)_{e} h^3 \frac{\partial p}{\partial y}\right] = 6(u_a + u_b)\frac{\partial \rho^* h}{\partial x}, \tag{3}$$

where $\left(\frac{\rho}{\eta}\right)_{es} = 12\left(l_s \frac{\rho_e}{A}\frac{\eta_e}{\eta_e'} + \left(\frac{h}{A}\eta_{z=0} - 1\right)\frac{\eta_e}{\eta_e'}\rho_e'\right)$, $\left(\frac{\rho}{\eta}\right)_{e} = 12\left(\frac{\eta_e}{\eta_e'}\rho_e' - \rho_e''\right)$, $A = h\eta_{z=0} + l_s\eta_e$, $\eta_e = h/\int_0^h \frac{1}{\eta} dz$,

$\eta_e^{'}=h^2/\int_0^h \frac{z}{\eta}dz$, $\rho_e=\frac{1}{h}\int_0^h \rho dz$, $\rho_e^{'}=\frac{1}{h^2}\int_0^h \rho \int_0^z \frac{1}{\eta}dz'dz$, $\rho_e^{''}=\frac{1}{h^3}\int_0^h \rho \int_0^z \frac{z'}{\eta}dz'dz$, $\rho^*=\frac{2}{u_a+u_b}\left[u_a\rho_e\text{-}(u_a\text{-}u_b)\eta_e\rho_e^{'}\rho_{es}\right]$, and $\rho_{es}=\frac{1}{A}\left(l_s\frac{\rho_e}{\rho_e^{'}}+h\eta_{z=0}\right)$.

Here, $(\rho/\eta)_{es}$ and ρ_{es} are the slip parameters. When $l_s=0$, $(\rho/\eta)_{es}=0$, and $\rho_{es}=1$, surface a is under the continuum boundary condition, and Eq. (3) turns into the generalized Reynolds equation [33].

The pressure boundary conditions for the Reynolds equation are:

$$\begin{cases} p = 0, \text{ at } x=x_{in}=x_{out},\ y=y_{out} \\ p \geq 0, \text{ at } x_{in}<x<x_{out},\ -y_{out}<y<y_{out} \end{cases} \tag{4}$$

where x_{in}, and x_{out}, y_{out} represent the start and end of the calculation domain, respectively.

Considering the surface deformation and geometry, the film thickness for point contact is given as:

$$h(x,y)=h_{00}+\frac{x^2}{2R_x}+\frac{y^2}{2R_y}+\frac{2}{\pi E'}\frac{p(x',y')}{\sqrt{(x\text{-}x')^2+(y\text{-}y')^2}}dx'dy'. \tag{5}$$

The load balance equation can be written as follows:

$$\iint p(x,y)dxdy = w. \tag{6}$$

Because the lubricant density and viscosity vary with the local pressure and local temperature, the Dowson and Higginson model [34] is used to express the density-pressure-temperature relationship, and the viscosity-pressure-temperature relationship is determined using the Roelands equation [35]:

$$\begin{aligned} \rho &= \rho_0\left[1+\frac{0.6\times10^{-9}p}{1+1.7\times10^{-9}p}\text{-}0.00065(T\text{-}T_0)\right] \\ \eta &= \eta_0\left\{(\ln\eta_0+9.67)\left[-1+(1+5.1\times10^{-9}p)^{Z_0}\left(\frac{T\text{-}138}{T_0\text{-}138}\right)^{-S_0}\right]\right\} \end{aligned} \tag{7}$$

where $Z_0=\frac{\alpha}{5.1\times10^{-9}[ln(\eta_0)+9.67]}$, $S_0=\frac{\beta(T_0\text{-}138)}{ln(\eta_0)+9.67}$.

The evolution of the temperature field is composed of the lubricant film and two bounding solids [36]. The energy equation of the lubricant film is:

$$c\left[\rho u\frac{\partial T}{\partial x}+\rho v\frac{\partial T}{\partial y}-\left(\frac{\partial}{\partial x}\int_0^z \rho u dz'+\frac{\partial}{\partial y}\int_0^z \rho v dz'\right)\frac{\partial T}{\partial z}\right]-k\frac{\partial^2 T}{\partial z^2} = -\frac{T}{\rho}\frac{\partial \rho}{\partial T}\left(u\frac{\partial p}{\partial x}+v\frac{\partial p}{\partial y}\right)+\eta\left[\left(\frac{\partial u}{\partial z}\right)^2+\left(\frac{\partial v}{\partial z}\right)^2\right] \tag{8}$$

The temperature boundary conditions for Eq. (8) are as follows.

$$\begin{cases} T(x=x_{in})=T_0,\ (u\geq 0) \\ T(x=x_{out})=T_0,\ (u\leq 0) \end{cases} \tag{9}$$

The energy equations of the two bounding solids can be written as:

$$\begin{cases} c_a\rho_a u_a\dfrac{\partial T}{\partial x}=k_a\dfrac{\partial^2 T}{\partial z_a^2} \\ c_b\rho_b u_b\dfrac{\partial T}{\partial x}=k_b\dfrac{\partial^2 T}{\partial z_b^2}\ . \end{cases} \tag{10}$$

The boundary conditions for Eq. (10) are as follows.

$$\begin{cases} T(x=x_{in})=T_0 \\ T(z_a=-d)=T_0 \\ T(z_b=d)=T_0 \end{cases} \tag{11}$$

At the solid–lubricant interface, the following continuity equations of heat flux,

$$\begin{aligned} k\frac{\partial T}{\partial z}\Big|_{z=h}&=k_b\frac{\partial T}{\partial z_b}\Big|_{z_b=0},\ T_{z=h}=T_{z_b=0}, \\ k\frac{\partial T}{\partial z}\Big|_{z=0}&=k_a\frac{\partial T}{\partial z_a}\Big|_{z_a=0},\ T_{z=0}=T_{z_a=0}+\Delta T, \end{aligned} \tag{12}$$

are applied to satisfy the no-slip boundary condition on surface *b*, and the temperature jump ΔT on surface *a* is taken as the thermal slip boundary condition.

3 **Numerical methods**

To facilitate programing and calculation, all of the governing equations were used in non-dimensionalized form. The dimensionless parameters have the following forms: $W=\frac{w}{E'R_x^2}$,

$U_0=\frac{u_0\eta_0}{E'R_x}$, $X=\frac{x}{a}$, $Y=\frac{y}{a}$, $Z=\frac{z}{h}$, $Z_{a,b}=\frac{z_{a,b}}{a}$, $\overline{d}=\frac{d}{a}$, $h_0=\frac{a^2}{R_x}$, $H=\frac{h}{h_0}$, $P=\frac{p}{p_H}$, $\overline{T}=\frac{T}{T_0}$, $U=\frac{u}{u_0}$, $U_{a,b}=\frac{u_{a,b}}{u_0}$, $\overline{\eta}=\frac{\eta}{\eta_0}$, $\overline{\rho}=\frac{\rho}{\rho_0}$, $l_s^*=\frac{l_s}{h_0}$, and $l_k^*=\frac{l_k}{h_0}$.

In the EHL calculation based on the Reynolds equation in Eq. (3), the pressure distribution and elastic deformation were solved using the multigrid method and the multi-level multi-integration technique, respectively [37]. To obtain the temperature distribution, a sequential column sweeping method [38] was employed to solve the energy equations of both the solids and the lubricant film. Considering the boundary conditions in the inlet and outlet regions, forward and backward marching processes were repeatedly executed under ZEV contact. An initial pressure field was applied to calculate the temperature field. Then, the pressure field was renewed based on the calculated temperature field, and the temperature field was updated using the renewed pressure field. By repeating the above two steps, convergence was achieved when the relative errors of the pressure, load, and temperature values were smaller than 1×10^{-5}, 1×10^{-4}, and 1×10^{-6}, respectively. All errors were checked at the finest grid level.

For the pure rolling contact, five grid levels with 256 nodes along the x- and y-directions at the finest grid level were applied in the calculation domain $-4.5a \le x \le 1.5a$, $-3a \le y \le 3a$. Therefore, the pressure boundary condition is adopted as $p = 0$ at $x = -4.5a = 1.5a$, $y = -3a = 3a$, and $p \ge 0$ at $-4.5a \le x \le 1.5a$, $-3a \le y \le 3a$. In the z-direction, eleven nodes were used in the film, and six non-equidistant nodes were adopted in each solid in each solid of d=3.15a in thickness. The calculation domain is $-3.15a \le z_a \le 0$ for solid a, $0 \le z_b \le 3.15a$ for solid b, and $0 \le z \le h$ for lubricant. The main input data are given in Table 1.

For the ZEV contact, semi-field calculation is adopted in y-direction. Four grid levels with 513 nodes along the x-direction and 197 nodes along the y-direction at the finest grid level were applied in the calculation domain $-3a \le x \le 3a$, $0 \le y \le 1.8a$. Therefore, the pressure boundary condition is $p = 0$ at $x = -3a = 3a$, $y = 1.8a$, and $p \ge 0$ at $-3a \le x \le 3a$, $0 \le y \le 1.8a$. The calculation

domain in the *z*-direction is same to that of the pure rolling case. The calculation parameters are listed in Table 2.

Table 1 Input data for pure rolling contact.

Density of glass, ρ_a, kg/m^{-3}	2500
Specific heat of glass, c_a, J/(kg·K)	840
Thermal conductivity of glass, k_a, W/(m·K)	0.78
Density of steel, ρ_b, kg/m^{-3}	7850
Specific heat of steel, c_b, J/(kg·K)	470
Thermal conductivity of glass, k_b, W/(m·K)	46
Density of lubricant, ρ_0, kg/m^{-3}	877
Specific heat of lubricant, c, J/(kg·K)	2000
Thermal conductivity of lubricant, k, W/(m·K)	0.14
Pressure viscosity coefficient, α, Pa^{-1}	2.4×10^{-8}
Viscosity of lubricant, η_0, Pa·s	1.365
Reduced elastic modules, E', Pa	1.17×10^{11}
Equivalent radius, R_x, m	0.0127
Applied load, w, N	50

Table 2 Input data for ZEV contact.

Density of steel, $\rho_{a,b}$, kg/m^{-3}	7850
Specific heat of steel, $c_{a,b}$, J/(kg·K)	470
Thermal conductivity of steel, $k_{a,b}$, W/(m·K)	46
Ambient density of lubricant, ρ_0, kg/m^{-3}	875
Specific heat of lubricant, c, J/(kg·K)	2000
Thermal conductivity of lubricant, k, W/(m·K)	0.14
Pressure viscosity coefficient, α, Pa^{-1}	2.2×10^{-8}
Ambient viscosity of lubricant, η_0, Pa·s	0.08
Thermal viscosity coefficient pf lubricant, β, K^{-1}	0.042
Reduced elastic modules, E', Pa	2.26×10^{11}
Ambient temperature, T_0, K	313
Equivalent radius, R_x, m	0.025
Applied load, w, N	31.6

4 Results and discussions

4.1 Pure rolling contact

To discuss the effects of velocity slip on the variations in the EHL lubricant film, a glass–steel contact was considered under the pure rolling contact, where velocity slip occurred on the glass surface. Since the two bounding surfaces moved with the same velocity under the pure rolling contact (Fig. 1 (a)), the temperature of the lubricant film increased negligibly. Therefore, the thermal slip at the solid–lubricant interface was neglectable in the thermal analysis. Notably, the modified Reynolds equation (Eq. (3)) without thermal slip was found to be consistent with the equation in Ref. [21].

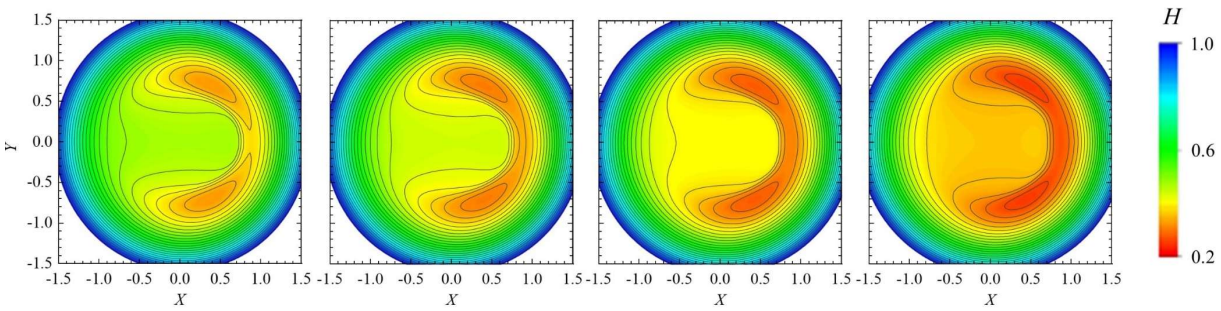

(a) $l_s^* = 0.0$ (b) $l_s^* = 0.063$ (c) $l_s^* = 0.157$ (d) $l_s^* = 0.314$

Fig. 2 Contour maps of lubricant film thickness under pure rolling contact at slip lengths of (a) $l_s^* = 0$, (b) $l_s^* = 0.063$, (c) $l_s^* = 0.157$, and (d) $l_s^* = 0.314$.

Fig. 2 shows the contour maps of the lubricant film thickness for $U_0 = 3.0 \times 10^{-10}$ with $l_s^* = 0$, 0.063, 0.157, 0.314. Here, l_s^* denotes the velocity slip according to the linear Navier slip condition. The employed slip length are in dimensionless forms, corresponding to 0.2 μm ($l_s^* = 0.063$), 0.5 μm ($l_s^* = 0.157$), and 1.0 μm ($l_s^* = 0.314$), respectively. These values of the slip lengths are comparable to EHL film thickness (approximate 1 μm). All of the contour maps exhibit a horseshoe shape of EHL contact, that is, a flat center plateau with two side lobes. In Fig. 2 (b), the small slip length of 0.063 does not induce an obvious difference in the film shape. As the slip length increases further, the central flat plateau is enlarged, while the minimum film

thickness in the side lobes decreases. Fig. 3 presents the pressure and film thickness profiles in the plane $Y = 0$ along the entrainment direction. The three locations *a, b,* and *c* are denoted as the inlet, center, and outlet of the contact region, respectively. As the slip length l_s^* increases, the pressure peak near location *b* shifts downward, and the second pressure peak close to location *c* shifts marginally upward, while the film thickness decreases significantly over the entire contact region.

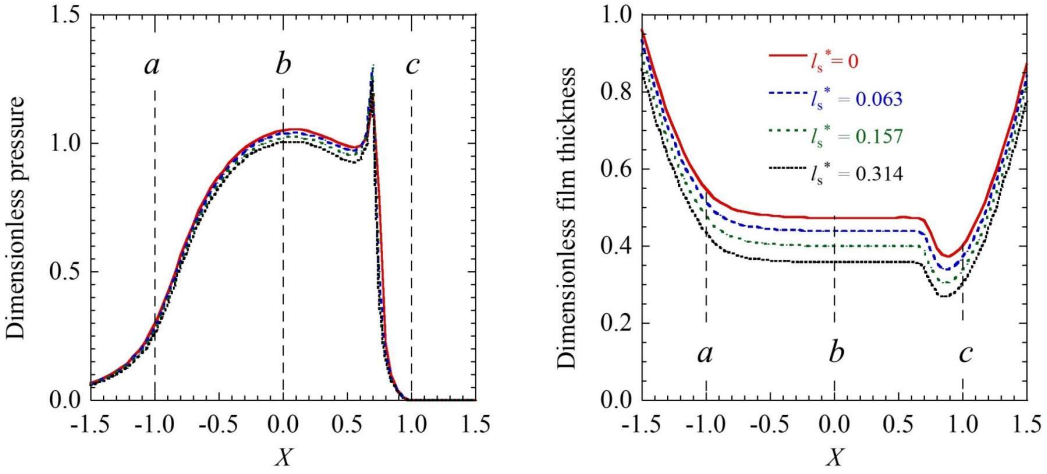

(a) Pressure (b) Film thickness

Fig. 3 Effect of slip length on (a) pressure and (b) film thickness at the plane $Y = 0$ under pure rolling contact.

Fig. 4 shows the lubricant velocity profiles across the lubricant film and the slip velocity at locations *a, b,* and *c*. As described in Fig. 1, velocity slip occurs on surface *a* ($Z = 0$), while surface *b* ($Z = 1$) is under the continuum boundary condition. At the inlet location *a* ($X = -1$, $Y = 0$), the velocity profiles across the lubricant film in the *z*-direction are hindered by the occurrence of velocity slip shown in Fig. 4 (a). As the slip length increases, the negative velocity gradient on the surface *a* ($Z = 0$) and the corresponding slip velocity U_s at location *a* increase monotonically, as shown in Fig. 4 (d). However, at location *b* ($X = 0$, $Y = 0$), the observed velocity profiles are linear and independent of the slip length. Thus, the velocity gradient is almost zero along the *z*-direction, resulting in zero slip velocity U_s, as shown in Fig. 4 (d). At

location c ($X = 1$, $Y = 0$), the shape of the lubricant velocity profile varies with the slip length. For $l_s^* = 0.314$, $U_{l_s^*=0.314} > U_{l_s^*=0}$ for $0 < Z \leq 0.4$, while the reverse is true for $0.4 < Z \leq 1.0$. The curve of U_s is quadratic at location c with a peak at $l_s^* \approx 0.2$, as shown in Fig. 4 (d). The existence of velocity slip on surface a decreases the entrainment velocity in the inlet region, which reduces the amount of lubricant entrained in the contact region. Consequently, the film thickness decreases, as shown in Fig. 3.

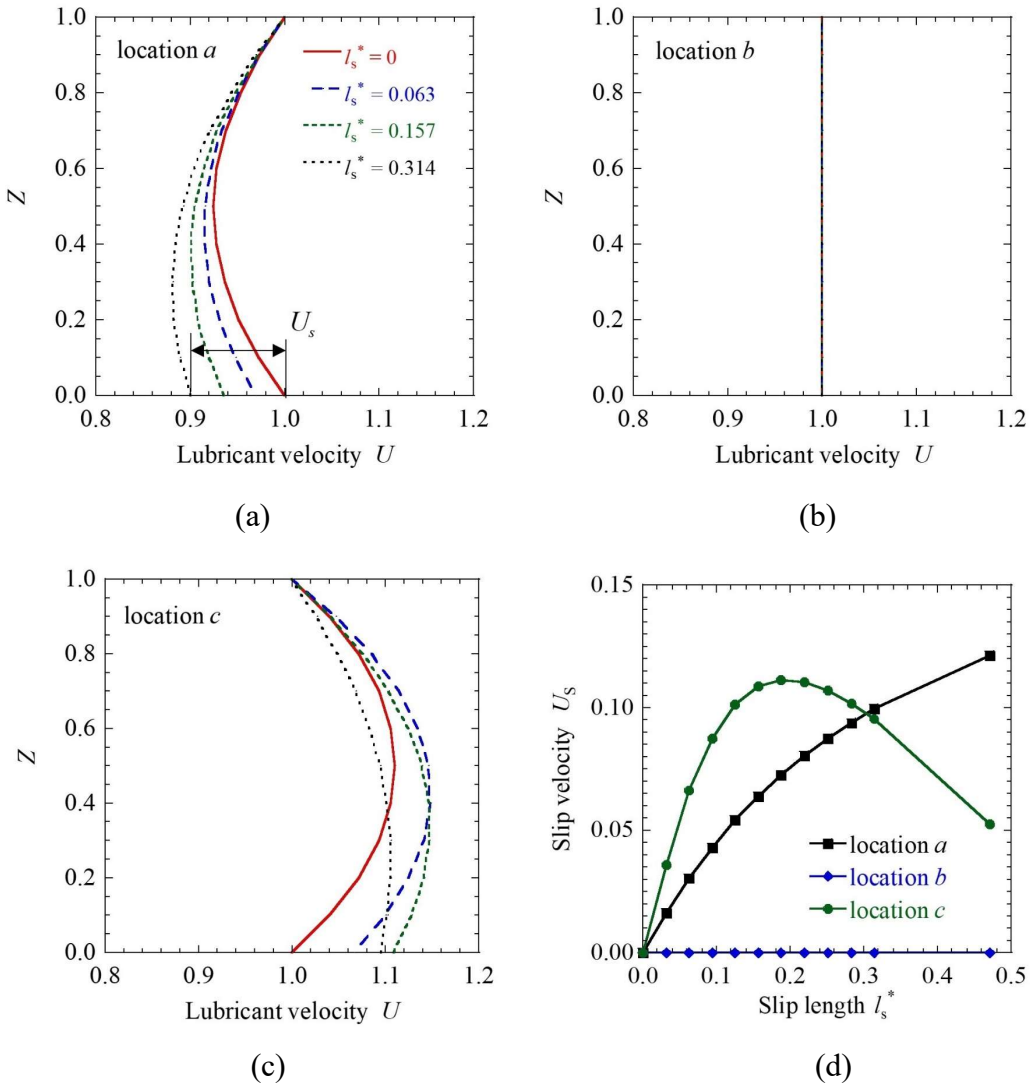

Fig. 4 Effect of slip length on (a–c) lubricant velocity distributions across lubricant film and (d) slip velocity at location a (X = -1, Y = 0), location b (X = 0, Y = 0), and location c ($X = 1$, $Y = 0$).

Fig. 5 describes the variations in the film thickness ratios corresponding to the increases in

entrainment velocity for different slip lengths. D_{cen} and D_{min} are the ratios of the center and minimum film thicknesses with velocity slip to those without velocity slip. Without the occurrence of velocity slip ($l_s^* = 0.0$), D_{cen} and D_{min} are always 1.0. According to Fig. 5, D_{cen} and D_{min} increase asymptotically as the entrainment velocity increases, indicating that the influence of slip length on film thickness in the low-velocity region is more apparent than that in the high-velocity region. For the same entrainment velocity, both D_{cen} and D_{min} decrease as l_s^* increases, while the value of D_{min} remains greater than that of D_{cen}. This means that the film thickness at the center is more significantly affected by the slip length than that in the side lobes.

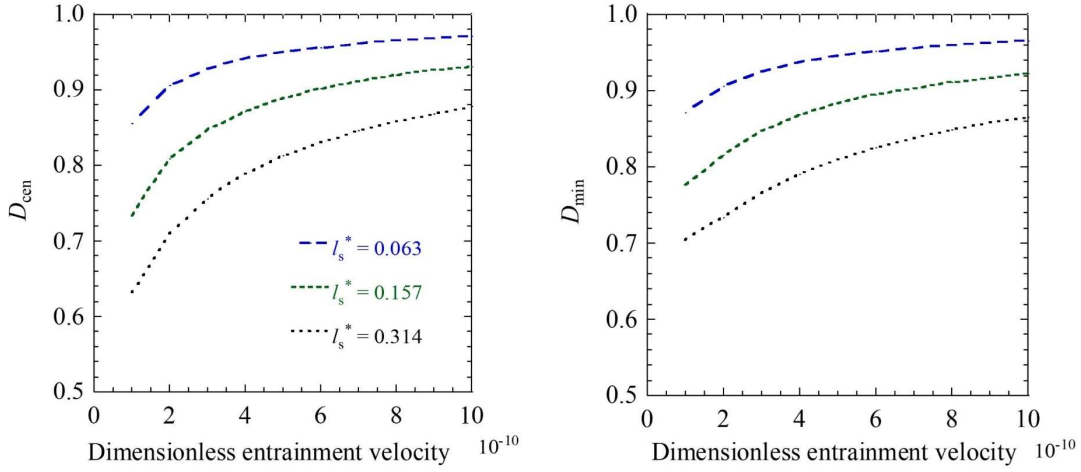

(a) Central film thickness (b) Minimum film thickness

Fig. 5 Effect of slip length on (a) central film thickness and (b) minimum film thickness with increasing entrainment velocity under pure rolling contact.

4.2 ZEV contact

In contrast to the abovementioned pure rolling contact (slide-roll ratio S = 0) in which two surfaces move in the same direction, ZEV contact involves two surfaces moving in opposite directions (for example, surface *a* moving from the left to the right, while surface *b* moving from the right to the left, as shown in Fig. 1 (b)) with the same speed (slide-roll ratio $S = \infty$). Thus, under ZEV contact, the temperature rise is expected to be more significant than that under

pure rolling contact in the same working conditions. On the other hand, the temperature rise also can be caused by reducing thermal conductivity. Habchi et al. [39], Reddyhoff et al.[40] and Liu et al. [41]. discussed the effects of the thermal conductivity on the EHL performance. To simplify the problem, the thermal conductivity of steel in its annealed/soft state is given as 46 W/(m·K), which is commonly used in literatures [24, 25, 29, 30].

This temperature increase is a dominant factor in maintaining a beneficial lubrication state, which is characterized by a surface dimple formed due to lubricant accumulation. Because the dimple is governed by the surface velocity and the subsequent temperature-viscosity wedge effect [29,30], the slip boundary condition may significantly influence the shape of the dimpled film. Here, the steel–steel ZEV contact shown in Fig. 1 (b) is employed to investigate the effects of the slip boundary condition on the lubrication performance, where the velocity/thermal slips occur on surface *a*.

4.2.1 Velocity slip effect

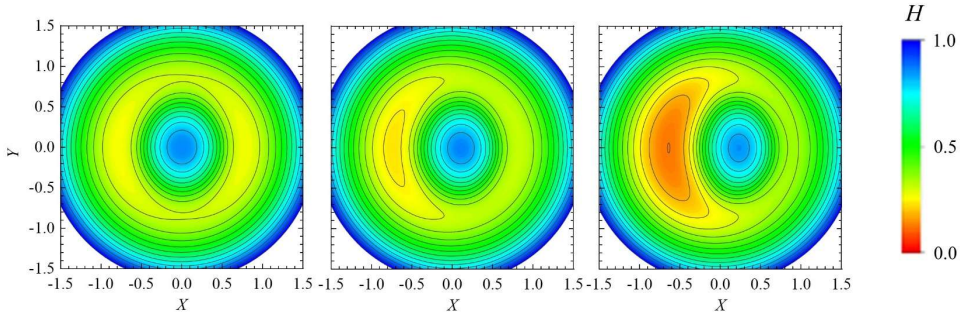

(a) $l_s^* = 0.0$ (b) $l_s^* = 0.02$ (c) $l_s^* = 0.04$

Fig. 6 Contour maps of lubricant film thickness under ZEV contact with $U_a = -U_b = 1.5$ and $l_k^* = 0$.

To simplify comparisons of the slip effects, the thermal slip length was set to zero ($l_k^* = 0$) in Figs. 6–9. Fig. 6 shows the contour maps of the lubricant film for $l_s^* = 0$, 0.02 and 0.04 with $U_a = -U_b = 1.5$. Under the no-slip boundary condition ($l_s^* = 0$), a large surface dimple is formed

in the contact area due to the temperature-viscosity wedge effect. As the slip length increases, the constriction in the left contact area is enlarged; consequently, the dimple is pushed toward the right side of the contact region. Fig. 7 shows the pressure and film thickness profiles in the plane $Y = 0$. Locations *a, b,* and *c* are denoted as the two sides and the center of the contact region, respectively. The pressure peak close to location *b* shifts toward the right side of the contact region (location *c*), and its magnitude increases as the slip length increases. The film thickness in the left side of the dimple thereby decreases, which squeezes the dimple toward the right.

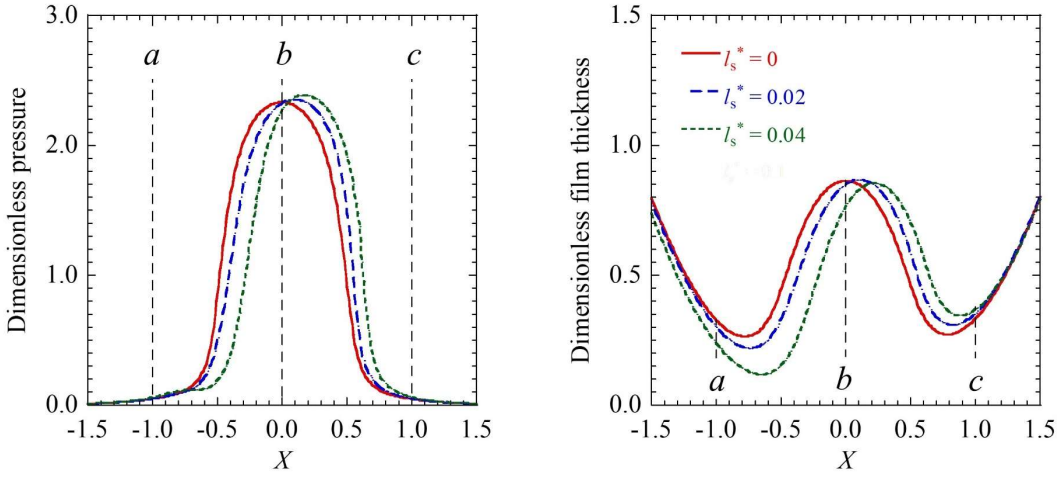

(a) Pressure (b) Film thickness

Fig. 7 Effect of slip length on (a) pressure and (b) film thickness in the plane $Y = 0$ under ZEV contact with $U_a = -U_b = 1.5$ and $l_k^* = 0$.

Fig. 8 shows the variations in lubricant velocity for $l_s^* = 0$, 0.02 and 0.04 across the lubricant film and the slip velocity at the three locations (indicated in Fig. 7). Larger slip length results in larger slip velocities at locations *a* and *c*, and smaller lubricant velocity, as shown in Figs. 8 (a) and (c). However, the slip velocity at location *b* is almost zero, and thus, the effect of slip length on lubricant velocity can be neglected at the center of the contact region. Since the absolute lubricant velocity near surface *a* is smaller than that near surface *b*, surface *a* drags less lubricant into the contact region than surface *b*. Therefore, the area of lubricant accumulation shifts from the center toward the right side of the contact region. Correspondingly,

the pressure peak and the surface dimple shift right.

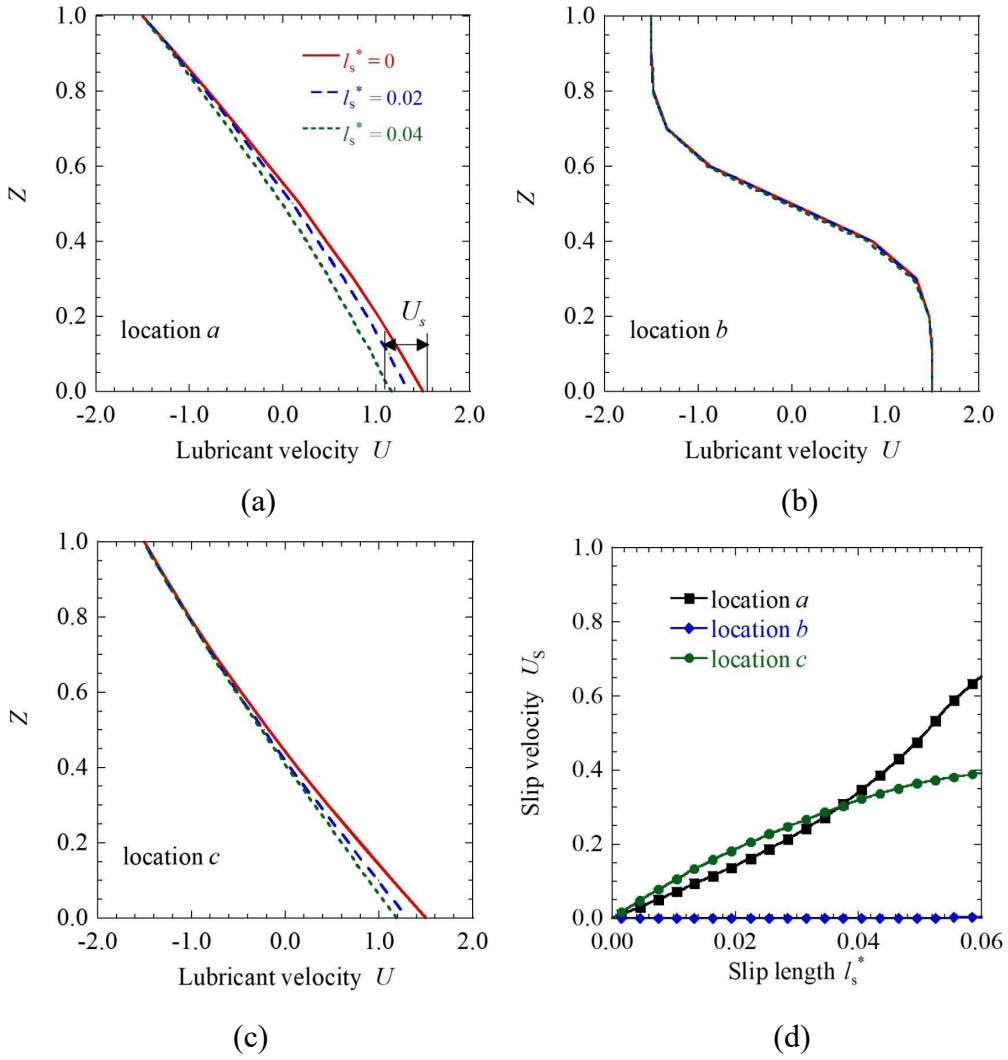

Fig. 8 Effect of slip length on (a–c) lubricant velocity distributions across the oil film and (d) slip velocity at location a ($X = -1$, $Y = 0$), location b ($X = 0$, $Y = 0$), and location c ($X = 1$, $Y = 0$).

Fig. 9 summarizes the maximum and minimum film thicknesses versus the slip length for three cases: $U_a = -U_b = 0.778$, 1.5, and 2.0. It is shown that both the maximum and minimum film thicknesses decrease as the slip length increases. Since hydrodynamic lubrication is accompanied with the EHL as the surface velocities U_a and U_b increase, the surface dimple is insignificant due to a reduction in elastic deformation [26], Thus, in the case of $U_a = -U_b = 0.778$, the maximum film thicknesses are the largest while the minimum film thicknesses are the smallest among the three cases. In Fig. 9 (b), the minimum film thicknesses decrease to

a constant value of 0.06 when the slip length is larger than a critical value in all of the three cases. The critical slip lengths are 0.03 for $U_a = -U_b = 0.778$, 0.05 for $U_a = -U_b = 1.5$, and 0.07 for $U_a = -U_b = 2.0$.

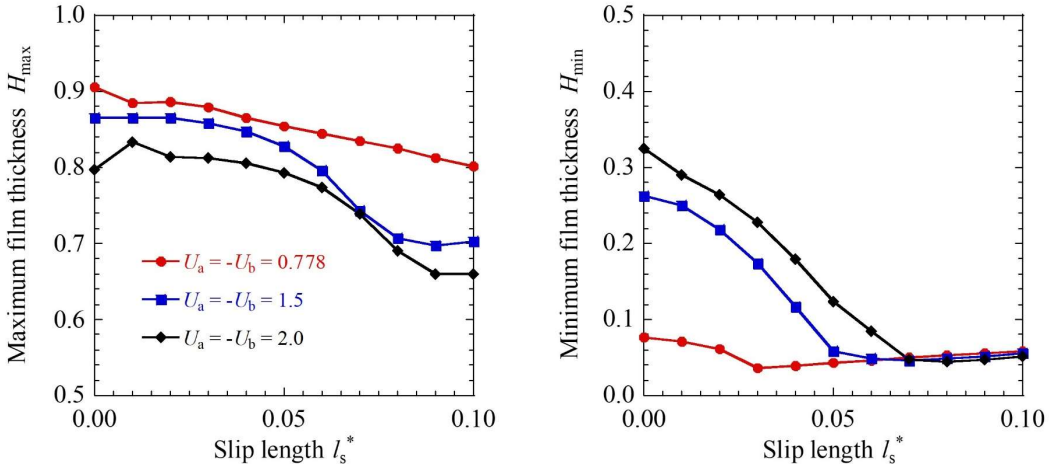

(a) Maximum film thickness (b) Minimum film thickness

Fig. 9 Film thickness variation with increase in slip length at $l_k^* = 0$.

An increase in temperature was found in the contact region due to the shearing and compression of the lubricant, consistent with previous studies [24–30]. The degree of the temperature rise is affected by the reduced lubricant velocity at surface *a*. The details of the shifted temperature profiles will be discussed in section 4.2.3.

4.2.2 Thermal slip effect

This section uses a slip length of zero ($l_s^* = 0$) to focus on the thermal slip effect. The film thickness contour maps are illustrated in Fig. 10 for $l_k^* = 0$, 0.02, and 0.04 with $l_s^* = 0$, $U_a = -U_b = 1.5$. In contrast to the results obtained in the previous section, the surface dimple moves toward the opposite direction, that is, toward the left side of the contact region under the thermal slip. Fig. 11 shows the pressure and film thickness profiles in the plane $Y = 0$ corresponding to Fig. 10. As the thermal slip length increases, the pressure peak and the surface dimple move toward the left from the center area, which is consistent with the film thickness contour maps shown in Fig. 10. Meanwhile, both the magnitude of the pressure peak and the dimple depth

decrease significantly at $l_k^* = 0.04$.

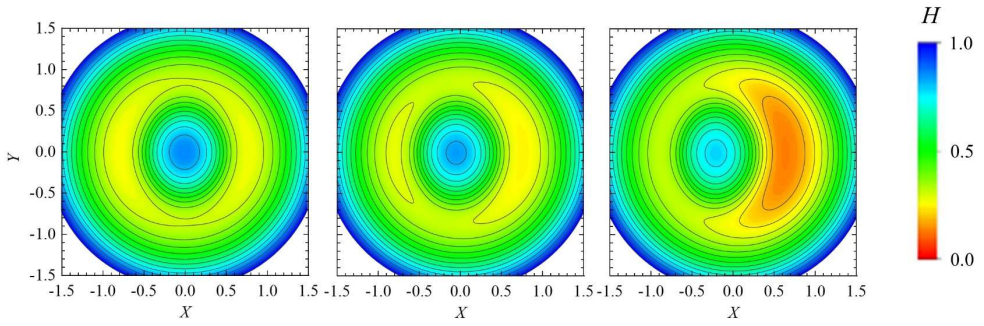

(a) $l_k^* = 0.0$ (b) $l_k^* = 0.02$ (c) $l_k^* = 0.04$

Fig. 10 Contour maps of lubricant film thickness under ZEV contact with $U_a = -U_b = 1.5$ and $l_s^* = 0$.

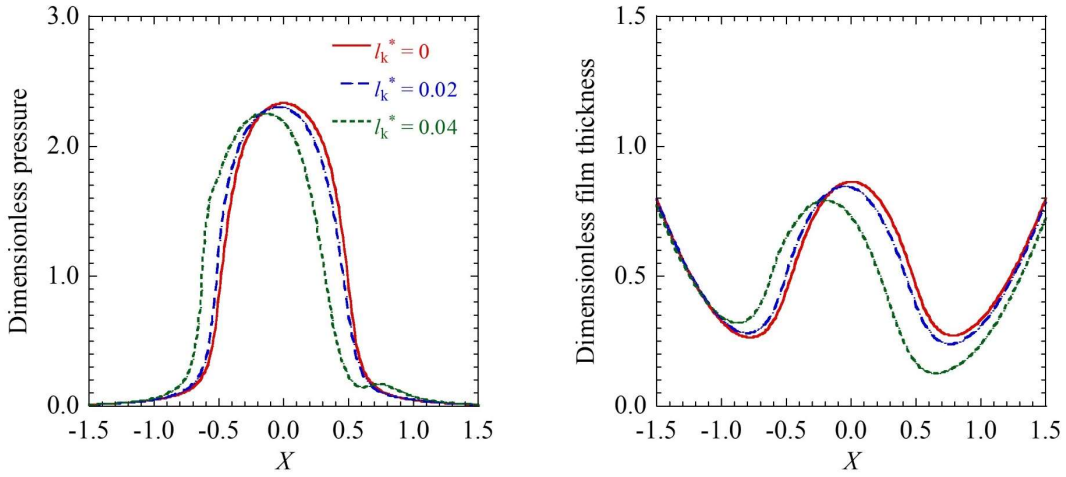

(a) Pressure (b) Film thickness

Fig. 11 Effect of thermal slip length on (a) pressure and (b) film thickness in the plane $Y = 0$ under ZEV contact with $U_a = -U_b = 1.5$ and $l_s^* = 0$.

Fig. 12 shows the temperature distributions along the *x*-*y* direction for $l_k^* = 0$, 0.02, and 0.04 on surface *a*. The temperature fields are non-uniform, and the temperature rise at $l_k^* = 0.04$ is the most prominent among the three simulation cases. The generated heat caused by shearing and compression of the lubricant is expected to dissipate through the lubricant and through surfaces *a* and *b*. However, the higher thermal resistance on surface *a* due to the increase in the thermal slip length limits heat dissipation from the lubricant to surface *a*. Thus, a significant temperature

rise occurs, induces a reduction in the lubricant viscosity. Consequently, a greater amount of lubricant is retained on surface *a* (moving right) at $l_k^* = 0.04$ than that at $l_k^* = 0$, which causes the accumulated lubricant to be pushed toward the left side of the contact region. Therefore, the surface dimples in Figs. 10 (b) and (c) move toward the left, which contradicts the dimple shift tendency in Fig. 7 caused by the velocity slip singularity.

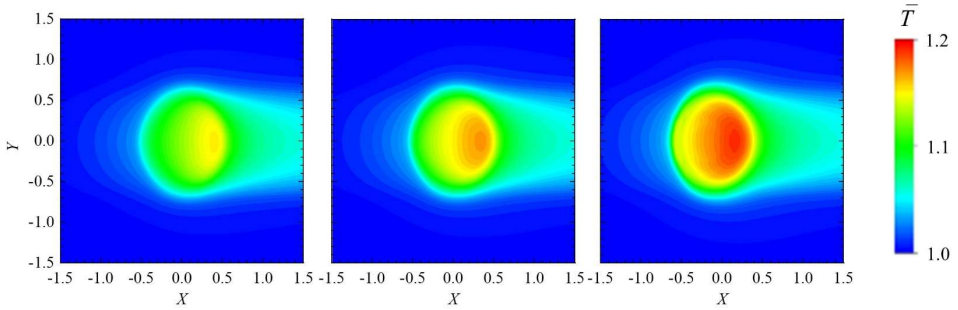

(a) $l_k^* = 0.0$ (b) $l_k^* = 0.02$ (c) $l_k^* = 0.04$

Fig. 12 Effects of thermal slip length on the temperature distributions on surface *a* under ZEV contact with $U_a = -U_b = 1.5$ and $l_s^* = 0$.

The variations in the maximum and minimum film thicknesses with the thermal slip length for $U_a = -U_b = 0.778$, 1.5, and 2.0 are shown in Fig. 13. Greater thermal slip length results in lower maximum and minimum film thicknesses. Notably, at $U_a = -U_b = 0.778$, the maximum film thickness decreases rapidly, while the minimum film thickness remains constant. In contrast, at $U_a = -U_b = 1.5$ and 2.0, the two extreme film thicknesses decrease in almost the same manner as the thermal slip length increases.

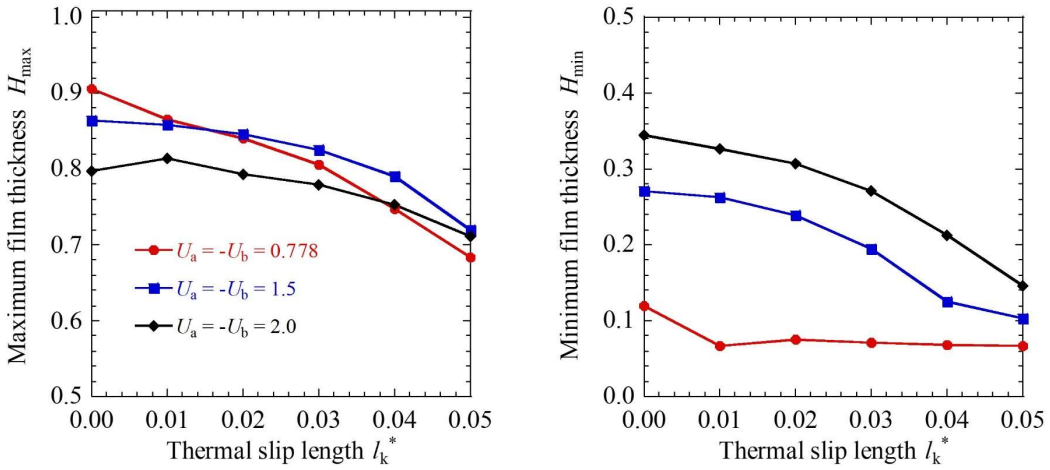

(a) Maximum film thickness (b) Minimum film thickness

Fig. 13 Film thickness variation with increase in thermal slip length under ZEV contact at $l_s^* = 0$.

4.2.3 Coupling thermal slip with velocity slip

In practice, the thermal slip and velocity slip could co-exist in lubrication region when slip boundary occurs. The thermal slip and velocity slip may be related; however, there is no guarantee that the velocity and thermal slips depend on each other [9, 10, 16, 17, 42]. The coupled effect of velocity slip and thermal slip on the lubrication performance is discussed in this section based on the individual investigations described in sections 4.2.1 and 4.2.2. Fig. 14 shows the temperature distributions inside the lubricant film in the plane $Y = 0$ for (a) no slip, (b) and (c) only velocity slip, (d) and (e) only thermal slip, (f) and (g) coupled velocity and thermal slips. As shown in Fig. 14 (a), the maximum lubricant temperature due to shearing and compression of the lubricant is at the center of the contact area, overlapping with the locations of the maximum pressure and surface dimple. A comparison among Figs. 14 (a), (b), and (c) shows that the location of the maximum temperature moves from the center toward the right as the slip length increases. By contrast, the increase of the thermal slip length causes the temperature-rise region to shift leftward, as shown in Figs. 14 (d) and (e). Unexpectedly, the effects of the coupled velocity slip and thermal slip ($l_s^* = l_k^*$) on the temperature distributions

cancel out one another, as shown in Figs. 14 (f) and (g), resulting in a similar temperature map as that in Fig. 14 (a).

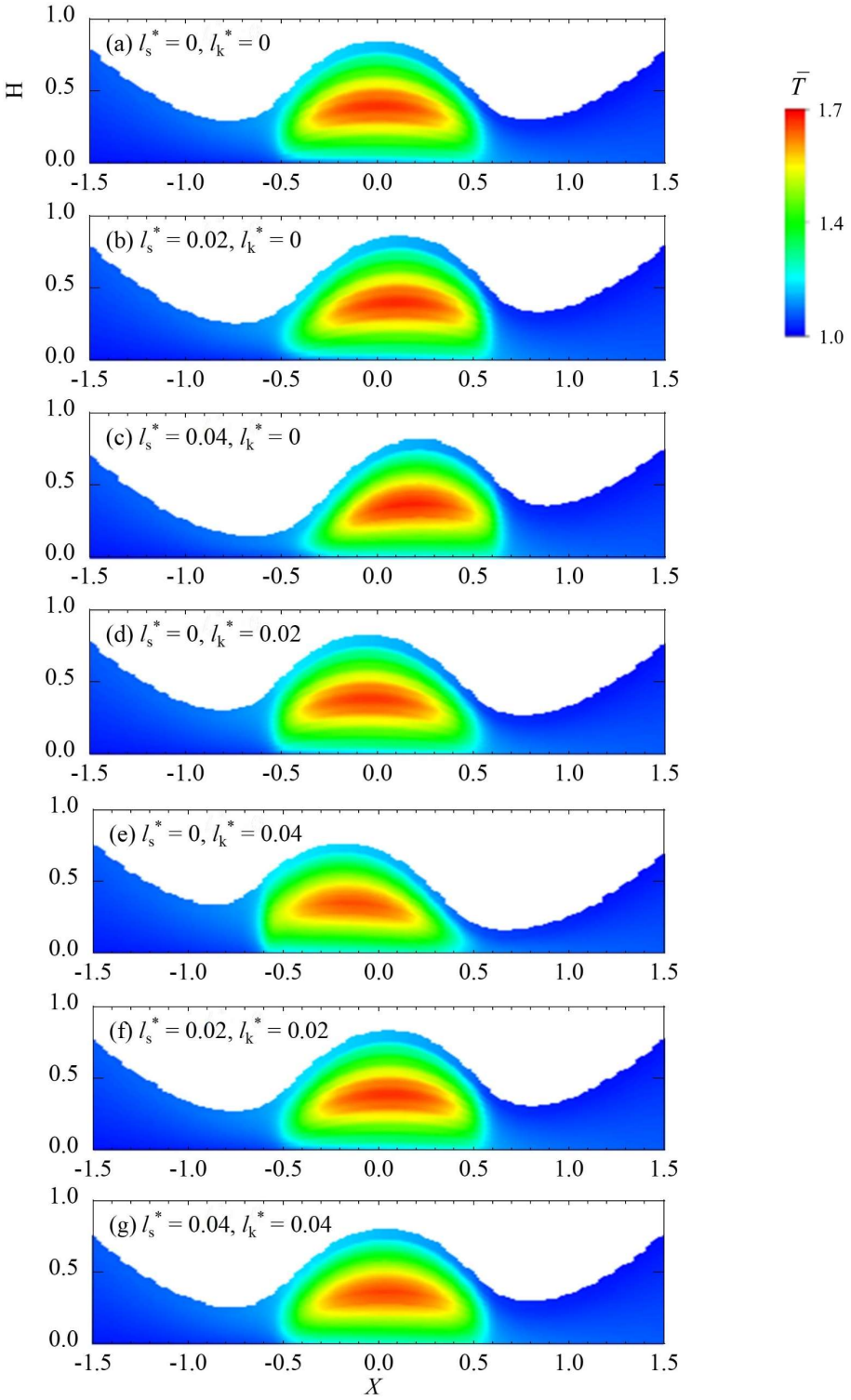

Fig. 14 Temperature distributions inside the lubricant film in the plane $Y = 0$ under ZEV contact with $U_a = -U_b = 1.5$.

In summary, the film thickness under ZEV contact can be significantly influenced by both velocity slip and thermal slip at the solid–lubricant interface due to the comparable scale of the slip lengths to the film thickness. However, the coupled effects of velocity and thermal slips cancel out one another when the slip length is comparable to the thermal slip length. Although the shape of the dimple changes slightly under the boundary slips for ZEV contact, the locations of the dimple, pressure peak, and temperature rise change remarkably. Because there is no guarantee that the slip length and the thermal slip length are comparable at a practical solid–lubricant interface, the effects of the coupled slips on the main factor (that is, either slip length or thermal slip length) should be carefully considered. When the slip length is the main factor, the lubrication features will follow the results presented in section 4.2.1. When the thermal slip length is the main factor, the lubrication features will follow the results presented in section 4.2.2.

In this study, the slip boundary condition was applied only on the sliding surface *a*. However, the slip boundary condition may occur on surface *b* or on surfaces *a* and *b*. Future works on boundary slips in EHL should be conducted with the aim of explaining the existing gap between the experimental results and the theoretical results.

5 Conclusions

The effects of boundary slip on the film thickness in point contact under pure rolling and opposite sliding contacts were investigated. Numerical simulations were conducted based on the modified Reynolds equation and the energy equation by considering the velocity slip and thermal slip simultaneously on a sliding surface. The following conclusions were drawn:

1. Under the pure rolling contact, velocity slip induced a lubricant velocity distribution across the film, which led to a general reduction in film thickness. The influence of velocity slip

on film thickness weakened as the entrainment velocity increased.

2. Under the ZEV contact, velocity slip caused the surface dimple to shift along the sliding direction, while thermal slip caused the surface dimple to shift in the opposite direction as the pressure peak shifted downward and the dimple depth decreased. The effects of velocity slip and thermal slip canceled out one another when the velocity slip length and thermal slip length were equal.
3. This study, for the first time, revealed the effect of thermal slip at the solid–lubricant interface on lubrication behavior, which might be one of the key parameters in EHL contact.

Acknowledgement

This work is partly supported by the Ministry of Education, Science and Culture of the Japanese Government through the Grant-in Aid for Scientific Research, Project No. 18H01385 and the Initiative for Realizing Diversity in the Research Environment by Ministry of Education, Culture, Sports, Science and Technology, Japan.

References

[1] Hamrock BJ, Dowson D. Ball bearing lubrication. The elastohydrodynamics of elliptical contacts. 1981.

[2] Gohar R, Cameron A. Optical Measurement of Oil Film Thickness under Elasto-hydrodynamic Lubrication. Nature 1963;200:458–9.

[3] Wedeven LD. Optical measurements of elastohydrodynamics in rolling-contact bearings. University of London, 1970.

[4] Lamb H. Hydrodynamics. 6th edition. C.U.P; 1932.

[5] Neto C, Evans DR, Bonaccurso E, Butt HJ, Craig VSJ. Boundary slip in Newtonian liquids: A review of experimental studies. Reports on Progress in Physics 2005.

[6] Thompson PA, Troian SM. A general boundary condition for liquid flow at solid surfaces. Nature 1997;389:360–2.

[7] Kapitza PL. The study of heat transfer in Helium II. Helium 4, 1971, p. 114–53.

[8] Pollack GL. Kapitza Resistance. Reviews of Modern Physics 1969;41:48–81.

[9] Nagayama G. Boundary conditions and microscale heat transfer at solid-liquid interface. Journal of the Heat Transfer Society of Japan 2011;50:29–36.

[10] Nagayama G, Matsumoto T, Fukushima K, Tsuruta T. Scale effect of slip boundary condition at solid-liquid interface. Scientific Reports 2017;7:1–8.

[11] Kaneta M, Nishikawa H, Kameishi K. Observation of wall slip in elastohydrodynamic lubrication. Journal of Tribology 1990;112:447–52.

[12] Wong PL, Li XM, Guo F. Evidence of lubricant slip on steel surface in EHL contact.

Tribology International 2013;61:116–9.

[13] Ponjavic A, Wong JSS. The effect of boundary slip on elastohydrodynamic lubrication. RSC Advances 2014;4:20821–9.

[14] Wang P, Reddyhoff T. Wall slip in an EHL contact lubricated with 1-dodecanol. Tribology International 2017;113:197–205.

[15] Ehret P, Dowson D, Taylor CM. On lubricant transport conditions in elastohydrodynamic conjunctions. Proceedings of the Royal Society A: Mathematical, Physical and Engineering Sciences 1998;454:763–87.

[16] Nagayama G, Cheng P. Effects of interface wettability on microscale flow by molecular dynamics simulation. International Journal of Heat and Mass Transfer 2004;47:501–13.

[17] Nagayama G, Tsuruta T, Cheng P. Molecular dynamics simulation on bubble formation in a nanochannel. International Journal of Heat and Mass Transfer 2006;49:4437–43.

[18] Wen S, Zhang Y. EHL performance of the lubricant with shear strength: Part i — boundary slippage and film failure. Tribology Transactions 2000.

[19] Chu LM, Lin JR, Li WL, Lu JM. A model for line-contact EHL problems-consideration of effects of navier-slip and lubricant rheology. Journal of Tribology 2012;134.

[20] Chen Q Da, Jao HC, Chu LM, Li WL. Effects of Anisotropic Slip on the Elastohydrodynamic Lubrication of Circular Contacts. Journal of Tribology 2016.

[21] Zhao Y, Wong PL, Mao JH. Solving coupled boundary slip and heat transfer EHL problem under large slide–roll ratio conditions. Tribology International 2019;133:73–87.

[22] Cameron A. Hydrodynamic Lubrication of Rotating Disks in Pure Sliding. A new Type

of Oil Film Formation. Journal of the Institute of Petroleum 1951;37:471–86.

[23] Cameron A. The Viscosity Wedge. A S L E Transactions 1958;1:248–53.

[24] Yang P, Qu S, Chang Q, Guo F. On the theory of thermal elastohydrodynamic lubrication at high slide-roll ratios - Line contact solution. Journal of Tribology 2001;123:36–41.

[25] Guo F, Yang P, Wong PL. On the thermal elastohydrodynamic lubrication in opposite sliding circular contacts. Tribology International 2001.

[26] Guo F, Wong PL, Yang P, Yagi K. Film formation in EHL point contacts under zero entraining velocity conditions. Tribology Transactions 2002.

[27] Yagi K, Kyogoku K, Nakahara T. Relationship between temperature distribution in EHL film and dimple formation. Journal of Tribology 2005;127:658–65.

[28] Meziane B, Vergne P, Devaux N, Lafarge L, Morales-Espejel GE, Fillot N. Film thickness build-up in zero entrainment velocity wide point contacts. Tribology International 2020;141:105897.

[29] Zhang B, Wang J, Omasta M, Kaneta M. Effect of fluid rheology on the thermal EHL under ZEV in line contact. Tribology International 2015;87:40–9.

[30] Zhang B, Wang J, Omasta M, Kaneta M. Variation of surface dimple in point contact thermal EHL under ZEV condition. Tribology International 2016;94:383–94.

[31] Wong PL, Zhao Y, Mao J. Facilitating effective hydrodynamic lubrication for zero-entrainment-velocity contacts based on boundary slip mechanism. Tribology International 2018;128:89–95.

[32] Zhao Y, Wong PL, Mao JH. EHL film formation under zero entrainment velocity condition. Tribology International 2018;124:1–9.

[33] Peiran Y, Shizhu W. A generalized Reynolds equation based on non-Newtonian flow in lubrication mechanics. Acta Mechanica Sinica 1990;6:289–95.

[34] Dowson D, Higginson GR. Elasto-hydrodynamic theory. 1977.

[35] Roelands C. Correlational Aspects of the Viscosity-Temperature Pressure Relationship of Lubricating Oils. PhD Thesis 1966:495.

[36] Yang P. Numerical analysis of fluid lubrication. National Defense Industry Press; 1998.

[37] Venner CH, Lubrecht AA. Multilevel methods in lubrication. Tribology Series 2000.

[38] Yang P, Rodkiewicz CM. On the numerical analysis to the thermoelastohydrodynamic lubrication of a tilting pad inclusive of side leakage. Tribology Transactions 1997.

[39] Habchi W, Bair S. The role of the thermal conductivity of steel in quantitative elastohydrodynamic friction. Tribology International 2020;142:105970.

[40] Reddyhoff T, Schmidt A, Spikes H. Thermal conductivity and flash temperature. Tribology Letters 2019;67:0.

[41] Liu HC, Zhang BB, Bader N, Poll G, Venner CH. Influences of solid and lubricant thermal conductivity on traction in an EHL circular contact. Tribology International 2020;146, 106059.

[42] Nagayama G, Kawagoe M, Tokunaga A, Tsuruta T. On the evaporation rate of ultra-thin liquid film at the nanostructured surface: A molecular dynamics study. International Journal of Thermal Sciences 2010;49:59–66.

Nomenclature

a	Radius of Hertzian contact area (m)
d	Thickness of solids a and b in z-direction (m), $d = 3.15a$
E'	Reduced elastic modulus (Pa)
h	Film thickness
h_0	Reference lubricant film (m) a^2/R_x
h_{00}	Rigid central film thickness (m)
l_s	Slip length (m)
l_k	Thermal slip length (m)
p	Film pressure (Pa)
p_H	Maximum Hertzian pressure $3w/(2\pi a^2)$
R_x, R_y	Equivalent radius in x and y directions (m)
S	Slide-roll ratio $S = 2(u_a - u_b)/(u_a + u_b)$
T	Temperature (K)
T_0	Ambient temperature (K)
ΔT	Temperature jump
u_0	Reference velocity (m/s)
u_a, u_b	Velocity of surfaces (m/s)
u_s	Slip velocity (m/s)
w	Applied load (N)
x, y	Horizontal coordinates (m)
X, Y	Dimensionless horizontal coordinates x/a, y/a
z, z_a, z_b	Vertical coordinates of film and solids (m)
Z_a, Z_b	Dimensionless vertical coordinates of solids z_a/a, z_b/a